

Optimisation of Greenhouse Insect Screening with Computational Fluid Dynamics

H. Fatnassi; T. Boulard; C. Poncet; M. Chave

INRA–URIH, 400, route des Chappes, BP 167, 06903 Sophia Antipolis, France; e-mail of corresponding author: boulard@sophia.inra.fr

(Received 29 March 2005; accepted in revised form 25 November 2005; published online 2 February 2006)

The effect on airflow and climate of greenhouse insect screening of a 1000 m² multi-span rose greenhouse was numerically investigated by means of a computational fluid dynamics (CFD) model, which included the dynamics, thermal and water vapour transfer between the crop cover and the greenhouse air. The numerical results were at first validated against air exchange rate data using a tracer gas (N₂O) technique collected in an experimental greenhouse. Using CFD facilities, these measurements were compared with simulated decay data issued from the numerical model of the greenhouse. Good agreement was found between experimental and numerical results for different wind speeds and directions. In a second stage, this numerical model was used to investigate the effects of greenhouse insect screening (anti-*Bemisia*) on natural ventilation and inside climate. The consequences of windward and leeward openings were studied together with the use of two insect screen types (anti-*Thrips* and anti-*Bemisia*). The main results are then discussed with respect to crop protection and climate control procedures, and it is shown that temperature and humidity rise due to insect screening can be balanced by simple arrangements of the system, such as wiser orientations of the roof vents and the use of additional side openings.

© 2005 Silsoe Research Institute. All rights reserved
Published by Elsevier Ltd

1. Introduction

Important progress has been achieved recently through the use of computational fluid dynamics (CFD) for the modelling of the greenhouse distributed climate, including at crop level (Boulard & Wang, 2002). The progress in the level of realism is also essential, as illustrated by recent simulations, which consider the dynamic action of the crop on the flow and the subsequent heat and mass exchanges in commercial size greenhouses. The most recent studies of Fatnassi *et al.* (2003) relate to multi-span greenhouses of half an hectare, and the effect of various structural elements such as the vents (Lee & Short, 2000) and different insect proof screens have been considered. The recent massive intrusion in France (2002–2003) of new insect pests, such as the white fly *Bemisia tabaci*, one of the worlds most important pest species, which transmits many viruses, has made necessary physical protection of greenhouse crops using insect proof nets. Yet, pressure drops induced by this protection on air movements

reduce the air exchange rates and dramatically increase inside temperature and humidity. How CFD use can lead to significant progress for greenhouse designs and climate control strategies is shown in this paper.

2. Materials and methods

2.1. Experimental arrangement

2.1.1. Site and greenhouse description

The experimental greenhouse was a 922 m² multi-span greenhouse erected in the INRA experimental centre of Sophia Antipolis in the south of France (43°36'44.9" N latitude, 07°04'40.4" E longitude and 125 m altitude). This four span greenhouse (4 by 9.6 m width, 24 m length and 5.9 m maximum height) was a Multclair 9600 model plastic (Filclair, Venelles, France) covered with a polyethylene film and divided into two independent compartments (three spans of 614 m² and one span of 307 m²). Its roof vent maximum opening reaches

Notation

A_l	discharge coefficient	T^*	reduced form of the temperature
C_D	drag coefficient	u	wind speed, m s^{-1}
C_F	non-linear momentum loss coefficient	u_{ref}	reference speed, m s^{-1}
C_p	specific heat of air, $\text{J kg}^{-1} \text{ } ^\circ\text{C}^{-1}$	u^*	reduced form of the horizontal component of air speed
C_w	wind effect coefficient	v	vertical component of air speed, m s^{-1}
C_ϕ	coefficient of source term equation	v^*	reduced form of the transverse component of air speed
G_{abs}	radiation absorbed in each mesh of the crop cover, W m^{-2}	w^*	reduced form of the vertical component of air speed
Gr	Grashof number	x,y,z	Cartesian space coordinates, m
H	total height of the cover, m	α	porosity
H_{Ro}	outside relative humidity, %	Γ	diffusion coefficient
h	vent opening height, m	ΔT	inside to outside temperature difference, $^\circ\text{C}$
I_{LA}	crop stand leaf area index	$\frac{\Delta T}{T}$	mean temperature difference, $^\circ\text{C}$
K	permeability of the porous medium, m	$\frac{\Delta \omega}{\omega}$	mean absolute humidity difference, kg kg^{-1}
K_c	the extinction coefficient of radiation, set to 0.75 for a tomato crop	ε	dissipation rate of turbulent kinetic energy, $\text{m}^2 \text{s}^{-3}$
k	turbulent kinetic energy, $\text{m}^2 \text{s}^{-2}$	λ	latent heat of water vapourisation, J kg^{-1}
N	greenhouse air exchange rate, h^{-1}	μ	dynamic viscosity of the fluid, $\text{kg m}^{-1} \text{s}^{-1}$
P	air pressure, Pa	ρ	air density, kg m^{-3}
Pr	Prandtl number of air	σ	standard deviation
Q_{lat}	latent heat exchange, W m^{-2}	ϕ	concentration of the transported quantity
Q_{sen}	sensible heat exchange, W m^{-2}	ϕ_o	value term
R_{gi}	global radiation inside the greenhouse, W m^{-2}	ω_a	absolute humidity of air, kg kg^{-1}
R_{go}	global radiation outside the greenhouse, W m^{-2}	ω_l^*	absolute humidity at saturation at leaf level, kg kg^{-1}
r_a	aerodynamic resistance of leaves, s m^{-1}		
r_s	stomatal resistance of leaves, s m^{-1}		
S_ϕ	source term		
T_a	air temperature, $^\circ\text{C}$		
T_l	temperature of the crop surface, $^\circ\text{C}$		
T_o	outside air temperature, $^\circ\text{C}$		
T_{ref}	reference temperature inside the greenhouse, $^\circ\text{C}$		
T_{so}	outside soil surface temperature, $^\circ\text{C}$		

Subscripts

T	temperature
ω	absolute humidity

1.8 m and rolling up side openings are positioned on its south, north and east sides. Anti-*Bemisia* insect proof nets (0.25 mm by 0.78 mm with 0.22 mm diameter wires) were installed on all the vent openings.

2.1.2. Measurement system

Air exchange rate measurements used to validate the CFD simulations were performed in this experimental greenhouse for various wind directions and speeds together with different vent opening configurations. Decay rate measurements with N_2O as tracer gas were achieved with an infrared N_2O analyser (Analytical Development Company; UK, 0–50 p.p.m full scale), and greenhouse air exchange rates were deduced from the decay rate of the inside N_2O concentration (Roy *et al.*, 2002).

2.2. Simulation

2.2.1. Fundamental computational aerodynamics

The fundamental calculation of the airflow pattern is based on computational aerodynamics using the mass, momentum and energy conservation equations. The three-dimensional conservation equations describing the transport phenomena for steady flows in free convection are of the general form

$$\frac{\partial(u^*\phi)}{\partial x} + \frac{\partial(v^*\phi)}{\partial y} + \frac{\partial(w^*\phi)}{\partial z} = \Gamma \cdot \nabla^2 \phi + S_\phi \quad (1)$$

where ϕ represents the concentration of the transported quantity in a dimensionless form, namely the three-dimensional momentum (Navier–Stokes) and the scalar mass and energy conservation equations; u^* , v^* and w^* are the reduced forms of the components of velocity

Table 1
Reduced form of the variables ϕ , diffusion Γ and source S_ϕ terms of the conservation equations for the mass, momentum (along X and Y) and energy terms

	ϕ	Γ	S_ϕ
Equation of mass	1	0	0
Equation of momentum (X)	$u^* = u/u_{ref}$	$1/Gr^{0.5}$	$-\partial P/\partial x$
Equation of momentum (Y)	$v^* = v/u_{ref}$	$1/Gr^{0.5}$	$\theta - \partial P/\partial y$
Equation of energy	$T^* = (T_a - T_{ref})/\Delta T$	$1/Pr Gr^{0.5}$	0

Gr , Grashof number; P , air pressure; Pr , Prandtl number of air; T_a , air temperature; T_{ref} , reference air temperature inside the greenhouse; T^* , reduced form of the temperature; ΔT , inside to outside temperature difference; u , wind speed; u_{ref} , reference speed; u^* , reduced form of the horizontal component of air speed; v , vertical component of air speed; v^* , reduced form of the transverse component of air speed.

vector; x, y, z are the Cartesian space coordinates; Γ is the diffusion coefficient; S_ϕ is the source term; and ∇^2 is the Laplace operator. These variables, with their diffusion, Γ , and source terms, S_ϕ , are shown in Table 1. The numerical code known as CFD codes solved the set (1) of highly non-linear equations using a spatial discretisation. As pointed out by turbulent air flow measurements in a greenhouse tunnel (Boulard *et al.*, 2000), inside air flows are highly turbulent, and turbulence models must be introduced in the set of equations. In this study, the closure procedure for turbulence modelling is the $k-\epsilon$ model (Launder & Spalding, 1972), which introduces two new phenomenological variables: the turbulent kinetic energy k and its dissipation rate ϵ [both can be considered in the form of Eqn (1)]. A complete set of the equations of the $k-\epsilon$ model can be found in Mohammadi and Pironneau (1994), and their commonly used parameters are given in the CFD 2000 manual (1997).

2.2.2. Interactions between air and crop cover

Dynamics

The sink of momentum due to the drag effect of the crop corresponds to the source term S_ϕ in Eqn (1). It can be expressed by unit volume of the cover by the commonly used formula (Wilson, 1985)

$$S_\phi = -I_{LA} C_D v^2 \quad (2)$$

where: v is air speed in m s^{-1} ; I_{LA} the leaf area density; and C_D a drag coefficient. In order to include a drag effect proportional to leaf density in our CFD study, the crop cover was considered as a porous medium and the Darcy–Forsheimer equation was used

$$S_\phi = ((\mu/K)v + (C_F/K^{0.5})v^2) \quad (3)$$

where: μ is the dynamic viscosity of the fluid in $\text{kg}^{-1} \text{m}^{-1} \text{s}^{-1}$; K the permeability of the porous medium in m ; and C_F the non-linear momentum loss coefficient. For the low air speed values observed in the crop cover, the first term of Eqn (3) can be neglected in front of the quadratic term. Combining Eqns (2) and (3) then yields

$$C_F/K^{0.5} = I_{LA} C_D \quad (4)$$

Sensible heat and water vapour exchanges. A last step in determining the true microclimatic picture at plant level involves the modelling of heat and water vapour exchanges between the leaves and air. This was performed by combining the porous medium approach to model dynamic effects and a macro-model of heat and mass transfer between the leaves and the air within each mesh of the crop cover (Haxaire, 1999; Boulard & Wang, 2002). The sink of momentum due to crop cover and the sensible and latent (crop transpiration) heat exchange between the crop cover and air must be considered in conjunction. Thanks to the possibility to customise CFD programs (Haxaire, 1999), the exchanges of heat and water vapour between leaves and air are introduced in the model. They are described by means of the heat and mass balances of leaves with the air [Eqns (5(a)–(c))] according to the big leaf approach. Each mesh of the crop cover is assimilated to a ‘volume heat source boundary condition’, receiving a net radiative flux G_{abs} in W m^{-2} [Eqn 5(a)], which is partitioned into convective sensible Q_{sen} and latent Q_{lat} heat fluxes in W m^{-2} (water vapour) according to the relations [Eqns (5(a)–(c))]. Within each mesh the sensible and latent heat exchange balance [Eqns (5(b) and (c))] depends on the values of the stomatal r_s and aerodynamic r_a resistances in s m^{-1} between the virtual solid matrix representing the crop and is characterised by its surface temperature T_l and the air T_a in $^\circ\text{C}$:

$$G_{abs} = Q_{sen} + Q_{lat} \quad (5a)$$

$$Q_{sen} = I_{LA} \rho C_P (T_l - T_a) / r_a \quad (5b)$$

$$Q_{lat} = \lambda I_{LA} \rho C_P (\omega_l^* - \omega_a) / (r_a + r_s) \quad (5c)$$

where: C_P is the specific heat of air at constant pressure in $\text{J kg}^{-1} \text{ } ^\circ\text{C}^{-1}$; ρ is the air density in kg m^{-3} ; λ is the latent heat of water vapourisation in J kg^{-1} ; ω_l^* and ω_a are the absolute humidity at saturation at leaf temperature and the absolute humidity of greenhouse air in kg kg^{-1} .

As r_a and r_s depend on the local computed air speed (u, v, w) and climatic conditions (T, ω), a close coupling is realised between the crop and air flow.

In addition, a new phenomenological variable, the temperature of the crop surface T_b and an additional

output of great interest, the transpiration of the cover Q_{lat} , are also available for each mesh of the crop cover. *Radiation absorption in the crop cover.* The radiation, G_{abs} , absorbed in each mesh of the crop cover of ordinates y_1 and y_2 can be directly deduced from the Beer law giving radiation transmission at height y in a porous medium:

$$G(v) = R_{gi} \exp(-K_c I_{LA}(H - y/H)) \quad (5d)$$

$$G_{abs} = G(y_1) - G(y_2) \quad (5e)$$

where: R_{gi} is the global radiation inside the greenhouse in $W m^{-2}$, K_c is the extinction coefficient of radiation, set to 0.75 for a tomato crop; H is the total height of the cover in m; and I_{LA} is the crop stand leaf area index.

2.2.3. Computational fluid dynamics package

The numerical solution was made possible by use of a finite volume discretisation code with the pressure implicit with splitting of operators (PISO) algorithm (CFD2000[®] manual, 1997). The driving force of the natural convection is the buoyancy force arising from small temperature differences within the flow according to the Boussinesq hypothesis, and a standard equation $k-\epsilon$ model assuming isotropic turbulence was used to describe the turbulent transport, this choice being a good compromise for a realistic description of turbulence and computational efficiency (Jones & Whittle, 1992). On average, 5 days were necessary before converging to a solution for each trial using a 2.5 GHz frequency computer with a 512 MB random access memory (RAM).

2.2.4. Computational fluid dynamics customisation

The CFD program was customised in Fortran in order to perform the balance described by Eqns 5(a)–(c), based on the local computed air speed and climatic conditions within each mesh of the porous medium (crop cover). These transfers were simulated using the Source model of CFD2000[®] software with a relation of the form:

$$S_\phi = C_\phi(\phi_o - \phi) \quad (6)$$

where: ϕ_o is a value term; C_ϕ is a coefficient; and ϕ is a dependent variable. For crop cover, ϕ refers to air temperature and humidity values within each mesh of the cover, ϕ_o to leaves temperature and humidity values within each mesh of the cover, and C_ϕ to the various exchange coefficients involved in Eqns 5(a)–(c).

2.2.5. Mesh and boundary conditions

Limits of the computational domain included (Fig. 1) the four spans greenhouse (only three spans are occupied with a rose crop and the unoccupied fourth span is separated from the other spans by a continuous

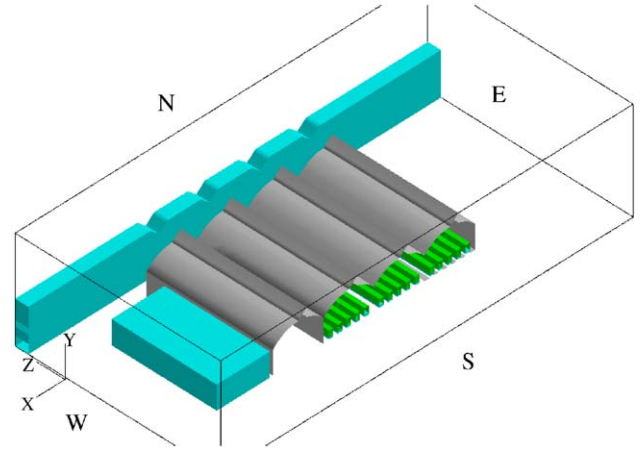


Fig. 1. Schematic view of the greenhouse, with the rose rows (porous medium in green colour) and its surroundings: a hedge to the north (porous medium in blue colour) and a low building (blockage in blue colour) in the west

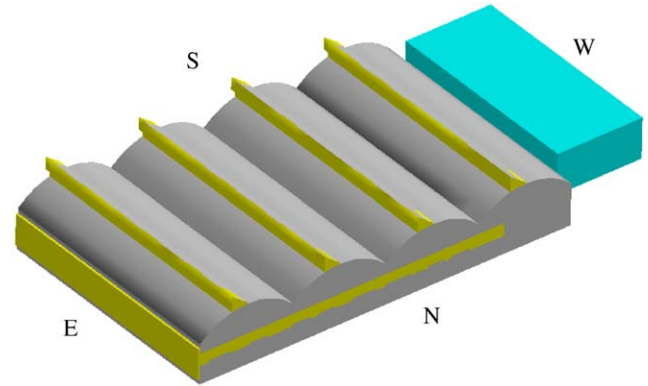


Fig. 2. Scheme of the nets (yellow colour) on the different openings of the greenhouse

plastic sheet), a building coupled to the greenhouse, considered as a blockage, and a cypress hedge situated on the north side of the greenhouse, considered as a porous medium. Inside the greenhouse, the rose rows were also considered as porous media, with the same geometry as in reality. The insect proof nets protecting the side and roof openings (Fig. 2) were considered as porous media with a larger thickness than in reality, but with a similar air transfer property (Table 2), in order to keep the same pressure lost while avoiding any size discontinuity in the meshing of the domain (Fatnassi, 2001). The computational grid of the CFD software used Cartesian coordinates, and a finer resolution was imposed in critical portions of the flow subject to strong gradients (wall boundary layers and in the mixing regions). Body-fitted coordinates were applied to exactly conform the grid to the contours of the greenhouse

Table 2
Dynamic and geometric characteristics of the anti-insects nets

Net	Mesh length, mm	Mesh width, mm	Wire diameters, mm	Porosity (α)	Permeability (K), m	Pressure loss coeff. (C_F)
Anti- <i>Bemisia</i>	0.78	0.25	0.22	0.41	8.26×10^{-10}	0.28
Anti- <i>Thrips</i>	0.18	0.18	0.22	0.2	2.67×10^{-10}	1.29

Table 3
Outside climate boundary limit conditions considered for the simulation

Air temperature (T_o), °C	Air relative humidity, (HR_o), %	Soil surf temp. (T_{so}), °C	Wind speed (u), $m s^{-1}$	Solar radiation (R_{go}), $W m^{-2}$
33	40	41	2.53	900

structure and boundary conditions. After several trials with different densities, the calculations were based on a 248 by 56 by 240 grid. It results from an empirical compromise between a dense grid, associated with a long computational time, and a less dense one, associated with a marked deterioration of the simulated results.

Measured climate conditions in summer for air velocity, temperature and humidity profiles in the windward limit of the domain were taken as boundary conditions and measured temperatures were applied to all wall boundaries (Table 3). Outlet boundary conditions were automatically computed to satisfy the continuity conditions. The inlet velocity profile was deduced from the measured wind profile fitted on the logarithmic profile following the formula found by Haxaire (1999) for the local (Mistral) wind:

$$u(y) = 0.45 \ln(y/0.0195) \quad (7)$$

where $u(y)$ is the wind speed at height y in m, *i.e.* $2.53 m s^{-1}$ at roof height. An empirical profile of turbulence was also imposed at the inlet following the formulas proposed by Scruton (1981).

2.2.6. The greenhouse crop system parameters

The porous medium approach described by Eqn (3) and available in the CFD software (CFD2000[®] manual, 1997) was used to model the dynamic effect of the crop cover on the flow. The parameters K and C_F involved in Eqn (3) were deduced from Eqn (4) with values for C_D of 0.32 (Haxaire, 1999; Boulard, 2004) and I_{LA} of 3. Values for K and C_F were deduced and used in relation to Eqns (3) and (4) to model the dynamics of air within the porous medium. The porous medium corresponded to the limits of the row crops: parallelepipeds 2 m high, 0.4 m wide and 18 m long. Heat and mass exchange between air and the row crops was governed by Eqns 5(a)–(c), with transfer resistances deduced from Boulard

et al. (1991) for stomatal resistance (varying with temperature, humidity and the net absorbed radiation inside each mesh of the porous medium) and Boulard *et al.* (2002) for aerodynamic resistance (varying with air speed inside each mesh of the porous medium).

2.2.7. Decay rate simulation

Once the convergence of the CFD model was obtained, decay rate simulations were performed using N₂O as tracer gas. For that, we have added a new variable to our model, the N₂O concentration, in addition to the commonly used variables (air speed vector, k , ε , air humidity, air temperature). Our model was then restarted with initial conditions corresponding to the converged solution for the commonly used variables and, in addition, with computation of N₂O transfers. The initial inside N₂O concentration value was set to 50 p.p.m and computer computation was interrupted every 10 s (simulated time), and the mean inside N₂O concentration observed. The decay rate of the inside N₂O concentration can then be deduced from the observed values, and a whole greenhouse air exchange rate can be calculated (Fernandez & Bailey, 1992).

3. Results

The dynamic and geometric characteristics of the anti-insects nets used for this study are recapitulated in Table 2. Let us recall that the experimental greenhouse was equipped with anti-*Bemisia* nets and that simulations were performed with such nets for model validation and anti-*Thrips* nets for purely simulation studies. For all the simulated cases, similar climate boundary conditions were adopted, representative of the prevailing average climate conditions (air temperature and humidity, wind speed and global radiation) at noon in July in South France; they are summarised in Table 3. Only East and

West wind directions were considered, and for both situations wind direction was considered as perpendicular (leeward or windward) to the roof vent opening surface.

3.1. Validation with respect to greenhouse air exchange rate performances

In order to validate the air exchange rate deduced from the model calculations, real air exchange rate measurements using N_2O as tracer gas were performed in the experimental greenhouse for different roof and side openings characteristics and two wind directions. The different configurations that were tested are summarised in Table 4. For all cases, the greenhouse was screened with anti-*Bemisia* nets and the roof openings were at the maximum (1.5 m height).


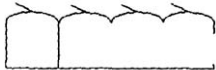

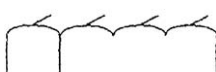
Considering all the measurements corresponding to various vent openings and wind directions, one (Bailey, 2000) can relate air exchange rate in $m^3 s^{-1}$ to vent opening surface in m^2 times the wind speed in $m s^{-1}$ and an average wind efficiency coefficient ($A_l C_w^{0.5}$) equal to

the product of the vent opening discharge coefficient A_l with the root square of the wind effect coefficient $C_w^{0.5}$ and equal here to 0.03. With respect to previous measurements (Bailey, 2000; Boulard & Baille, 1995) in multi-span greenhouses and tunnels, the identified value for the wind efficiency coefficient seems to be very low. It seems to be due to (i) the presence of anti-*Bemisia* nets on the openings and also (ii) to the presence of a partition inside the greenhouse, which hinders air circulation between the different vent openings. Comparison of measured and calculated (using CFD) air exchange rates for the same vent openings and outside climate characteristics (including wind direction and speed) highlights (Table 4) the rather good precision of the air exchange rate computations using the CFD simulations (standard deviation of $2.7 h^{-1}$).

3.2. Exploration of inside climate and air movements

Details of air speed, temperature and humidity patterns in a transverse vertical section of the greenhouse equipped with anti-*Bemisia* nets on the roof and

Table 4
Air exchange rate measurements using N_2O decay rate

(1) West roof opening	N, h^{-1} $u, m s^{-1}$ Wind dir. Wind dir. versus roof opening	13.7 6.7 0 P	13.7, 12.1 6.7 0.2 P	14.3 8.6 0.3 P	W E 
(2) West roof opening and side opening	N, h^{-1} $u, m s^{-1}$ Wind dir. Wind dir. versus roof opening	14.6 8.5 0.1 P	28.0, 21.1 7.1 0.2 P		W E 
(3) East roof opening and side opening	N, h^{-1} $u, m s^{-1}$ Wind dir. Wind dir. versus roof opening	13.7, 10.3 5.9 0.1 P	16.9 5.8 2.3 WW	14.8 3.6 0.6 LW 16.1 5.7 1.2 LW	W E 
(4) East roof opening	N, h^{-1} $u, m s^{-1}$ Wind dir. Wind dir. versus roof opening	5.2, 6.0 3.9 0.3 P	6.9 3.2 2.2 WW	2.3 3.6 0.3 P 4.4 5.5 1 LW	W E 
	N, h^{-1} $u, m s^{-1}$ Wind dir. Wind dir. versus roof opening	1.1 0.23 1.4 LW			

Notation conventions for wind direction: 0, N; 1, NE; 2, E; 3, SE; 4, S; 5, SW; 6, W; 7, NW.

Conventions for wind direction with respect roof openings: P, wind roughly parallel to the roof openings; WW, wind roughly windward to the roof openings; LW, wind roughly leeward to the roof openings. For four cases, the simulated air exchange rate values N corresponding to the same vents & wind conditions are indicated in bold characters. u wind speed.

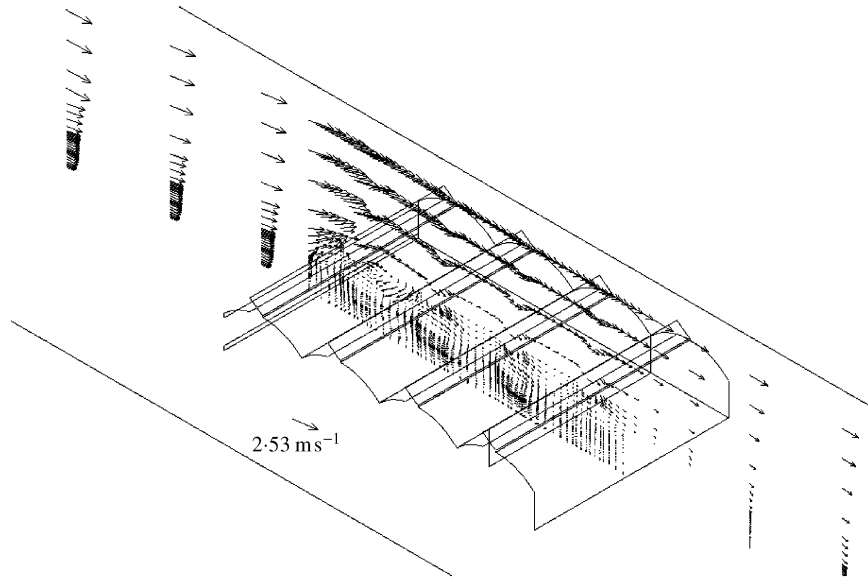


Fig. 3. General circulation of air around the greenhouse with anti-Bemisia nets on the vents in three dimensions (3D) in a section perpendicular to the vent openings

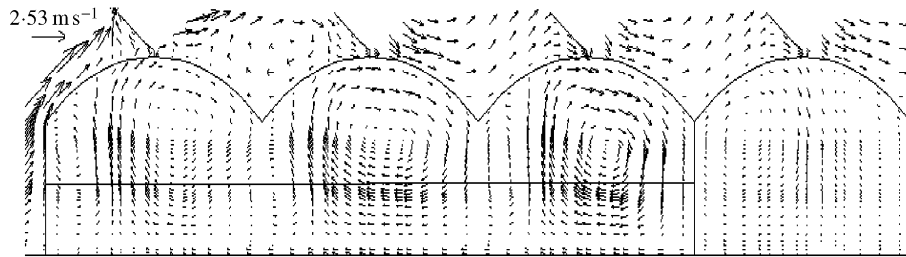


Fig. 4. Two dimensional dynamic field (in a section perpendicular to the vent openings) within the greenhouse for the configuration with open windward and side openings and with anti-Bemisia nets on the vents (inside horizontal line refers to crop height)

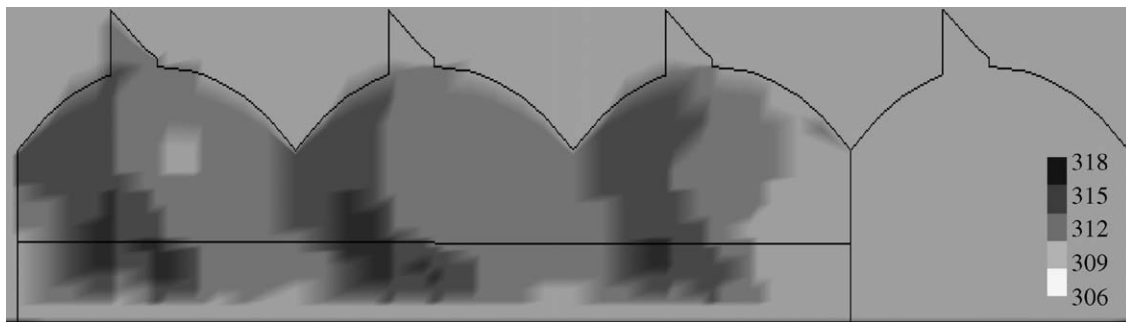


Fig. 5. Air temperature field in K within the greenhouse for the configuration with open windward and side openings and with anti-Bemisia nets on the vents (inside horizontal line refers to crop height)

side vents can be found in *Figs 3 and 4* for a wind direction perpendicular to the vents opening surface. Four spans are represented, but as already specified before; the west span was unoccupied and separated from the others by an air-tight plastic partition. There-

fore, the climate patterns in the three cultivated (rose crop) East spans are considered. Pressure losses due to the anti-Bemisia net hinder air penetration through the windward roof openings and the side vent opening. Yet, convective cells can be observed in each span, fed both

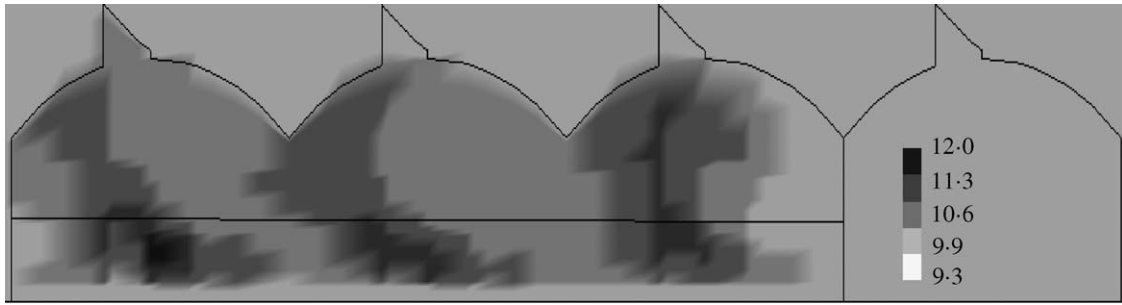


Fig. 6. Air humidity field in g kg^{-1} within the greenhouse for the configuration with open windward and side openings and with anti-Bemisia nets on the vents (inside horizontal line refers to crop height)

by air infiltrations through the screened vents and by buoyancy forces induced by the thermal and latent heat exchanges at screened vents and by buoyancy forces induced by the thermal and latent heat exchanges at crop level. Due to solar radiation absorption at crop level, plumes with higher air humidity and temperature can be observed above the row crops in each span, and one can also notice a general air circulation of cold air going from West to East below the tables supporting the rose plants (Figs 4–6).

3.3. Simulation study

3.3.1. Efficiency of the combination of roof and lateral vent openings

Efficiency of the combination of roof and lateral vent openings for, respectively, windward roof vents (cases 1 and 2 of Table 4) and leeward roof vents (cases 4 and 3 of Table 4) was studied by comparing simulated air temperature and humidity fields at 1 m high inside the greenhouse (Figs 5 and 6). For all cases, one can observe periodic climate variations due to the convective cells induced in each span (see details of inside flows in Fig. 4), together with a trend of temperature (Fig. 5) and humidity (Fig. 6) rise from the windward to the leeward side of the greenhouse. Comparison of the different vents *versus* wind situations (Figs 7 and 8) shows that the windward roof openings and side opening (case 2, Fig. 7) induces the minor temperature and humidity rise (mean temperature difference $\overline{\Delta T} = 2.7^\circ\text{C}$ with a standard deviation $\sigma_T = 2.1^\circ\text{C}$; mean absolute humidity difference $\overline{\Delta \omega} = 1.1 \text{ g kg}^{-1}$, $\sigma_\omega = 0.39 \text{ g kg}^{-1}$), and that the leeward roof opening (case 4, Fig. 8) cause the major one ($\overline{\Delta T} = 4.9^\circ\text{C}$, $\sigma_T = 2.2^\circ\text{C}$; $\overline{\Delta \omega} = 1.1 \text{ g kg}^{-1}$, $\sigma_\omega = 0.5 \text{ g kg}^{-1}$). Side openings do not significantly improve inside climate for windward roof openings (case 2, Fig. 7: $\overline{\Delta T} = 2.4^\circ\text{C}$, $\sigma_T = 1.4^\circ\text{C}$; $\overline{\Delta \omega} = 0.6 \text{ g kg}^{-1}$, $\sigma_\omega = 0.34 \text{ g kg}^{-1}$). Yet it reduces air temperature and humidity from 1.9°C and 0.33 g kg^{-1} for

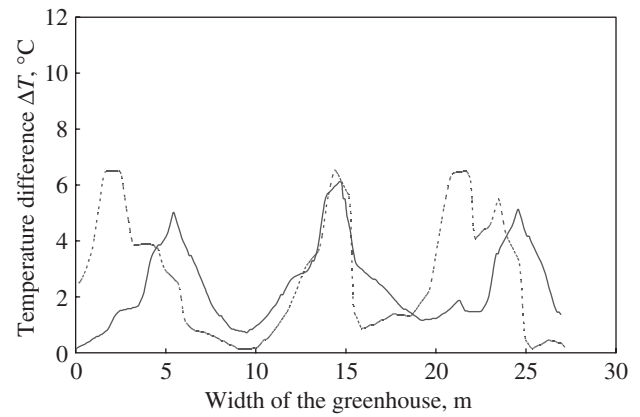


Fig. 7. Temperature difference between inside and outside: - - - windward openings only (1.5 m high); — windward openings (1.5 m high) and side opening

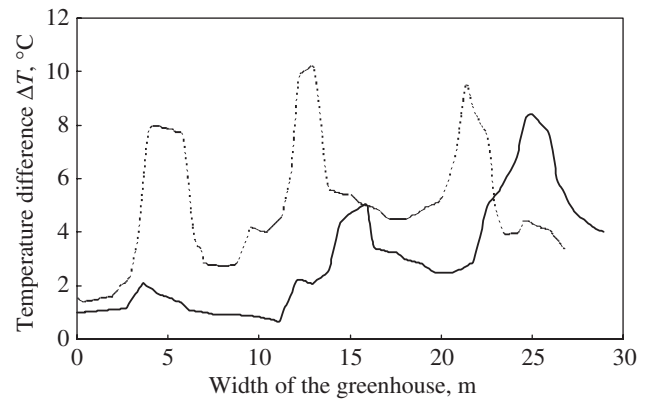


Fig. 8. Temperature difference between inside and outside: - - - leeward openings only (1.5 m high); —, leeward (1.5 m high) and side opening

leeward roof openings (case 3, Fig. 8), while still maintaining heterogeneous conditions ($\sigma_T = 2.1^\circ\text{C}$, $\sigma_\omega = 0.77 \text{ g kg}^{-1}$) (Table 5).

Table 5
Mean and standard deviation values for temperature and humidity difference between inside and outside

Openings	Mean temperature difference ($\overline{\Delta T}$), °C	Temperature standard deviation (σ_T), °C	Mean absolute humidity difference ($\overline{\Delta T}$), g kg ⁻¹	Absolute humidity standard deviation (σ_ω), g kg ⁻¹
Windward openings only (1.5 m high)	2.7	2.1	1.1	0.39
Windward (1.5 m high) and side openings	2.4	1.4	0.6	0.34
Leeward openings only (1.5 high)	4.9	2.2	1.1	0.5
Leeward (1.5 m high) and side opening	3.0	2.1	0.77	0.54
Windward (1.5 m high) and leeward (0.2 m high)	3.2	1.9	1	0.41
Windward (1.5 high), leeward (0.2 m high) and side opening	2.8	1.3	0.72	0.4

3.3.2. Efficiency of windward and leeward vent openings used together

It was assumed that, as commonly used in commercial greenhouses, both windward and leeward vents are open together, with a fully open (vent opening height $h = 1.5$ m) windward roof vent and a slightly open ($h = 0.2$ m) leeward one. This case was also studied alone, and combined with a lateral opening. Inside air temperature patterns obtained with these two last cases were compared [Figs 9(a) and (b)] with the previously studied cases without leeward roof openings (cases 1 and 2, respectively). It can clearly be seen that slightly opening (0.2 m) the leeward vent while maintaining the windward one fully open (1.5 m) induces a temperature rise of half degree. In case of combination with a lateral opening, the air temperature rise is quite similar (+0.4 °C). For both cases, we also note an air humidity elevation of +1.3 g kg⁻¹ and a quite similar climate heterogeneity (σ_T , σ_ω remain roughly unchanged). Thus, paradoxically, this study highlights that opening windward (1.5 m height) and leeward (0.2 m height) vents together is less efficient than opening the windward vent (1.5 m height) alone.

3.3.3. Effects of different types of insect screening on inside climate

Simulated climate condition inside the greenhouse without and with insect screens has been compared for the vent configuration corresponding to the combination of roof windward vents and lateral opening (case 2 of Table 4). We have considered inside air temperature with an anti-*Bemisia* protection and with an anti-*Thrips* protection (see nets characteristics in Table 1). Comparative profiles of inside air temperature elevation are given in Fig. 10 for these two cases, and the case without any insect protection and a recapitulative of the mean and standard deviation values for temperature and humidity are recapitulated in Table 6.

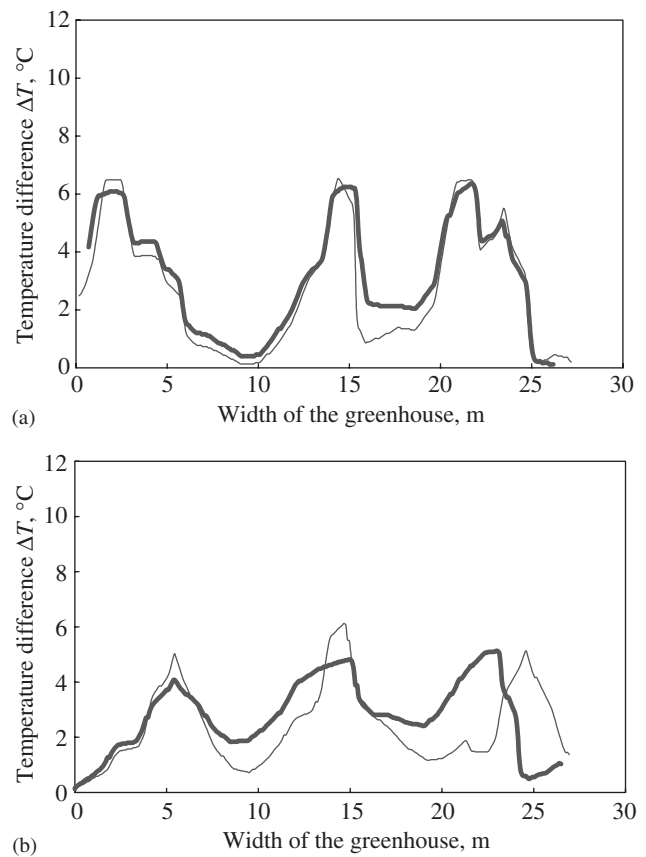


Fig. 9. (a) Temperature difference between inside and outside: —, windward openings only (1.5 m high); —, windward (1.5 m high) and leeward opening (0.2 m high). (b) Temperature difference between inside and outside: —, windward (1.5 m high) and side opening; —, windward (1.5 m high) and leeward (0.2 m high) and side openings

With respect to the case without any insect screening, anti-*Bemisia* nets generate quite an important air temperature and humidity rises (+2.7 °C and +0.7 g kg⁻¹) together with an increase in inside climate

heterogeneity. When compared to a compartment without any screen, air temperature and humidity rises with respect to outside are multiplied by two. For anti-*Thrips*

screens on the vents, air temperature and humidity rises are three times more important than without nets ($+4.7^{\circ}\text{C}$, $+1.3\text{ g kg}^{-1}$); details on the distributed air speed, temperature and humidity fields within the greenhouse are given in Figs 11–13.

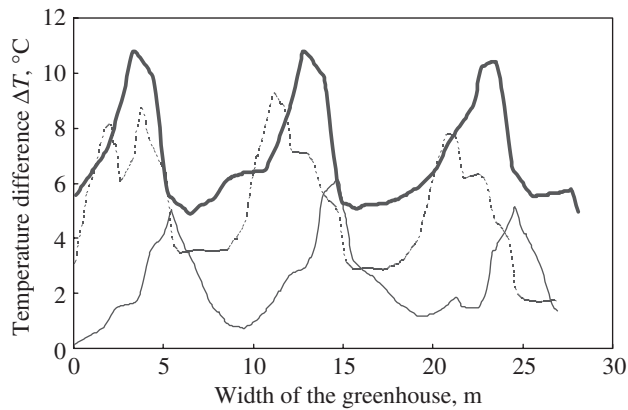


Fig. 10. Temperature difference between inside and outside: —, without nets on the openings; ----, with anti-*Bemisia* nets; —, with anti-*Thrips* nets; case with windward openings (1.5 m high) and side openings

Table 6
Mean and standard deviation values for temperature and humidity difference between inside and outside for the greenhouse without nets and with anti-*Thrips* and anti-*Bemisia* nets

Openings	Mean temperature difference (ΔT), $^{\circ}\text{C}$	Temperature standard deviation (σT), $^{\circ}\text{C}$	Mean absolute humidity difference (ΔT), g kg^{-1}	Absolute humidity standard deviation (σ_{ω}), g kg^{-1}
Anti- <i>Thrips</i> nets	7.1	1.8	1.9	0.3
Anti- <i>Bemisia</i> nets	5.1	2.1	1.2	0.47
Without nets	2.4	1.4	0.6	0.34

4. Conclusions

Combining greenhouse crops and air interactions by means of customised computational fluid dynamics (CFD) software notably improves the realism of these simulations. Thus, it offers the opportunity to use the numerical model for exploring the details of the inside air temperature and humidity patterns and accordingly for improving the greenhouse design and equipment quicker than with real scale prototypes. Maintaining a safe greenhouse insect screening and a fair inside climate is a challenging task, giving opportunity to test the applicability of this model-based approach.

Once validated with respect to greenhouse air exchange rate values, these simulations show that screened greenhouse ventilation and inside climate can substantially be improved by orienting roof vents windward rather than leeward. It is also clearly demonstrated that simultaneous windward and leeward roof vent opening does not improve ventilation and inside climate.

With respect to unscreened vents, anti-*Bemisia* net multiply both air humidity and temperature rises with respect to outside by a factor of 2 and by a factor of 3 for anti-*Thrips* nets. In this case, only additional opening surfaces combined with shadowing techniques and natural (crop based) or artificial (fog system) cooling systems can allow to maintain temperature and humidity conditions in a range favourable to plant growth. It could then be possible to apply a similar approach to study the combination of these methods and their influence on greenhouse ventilation and inside climate.

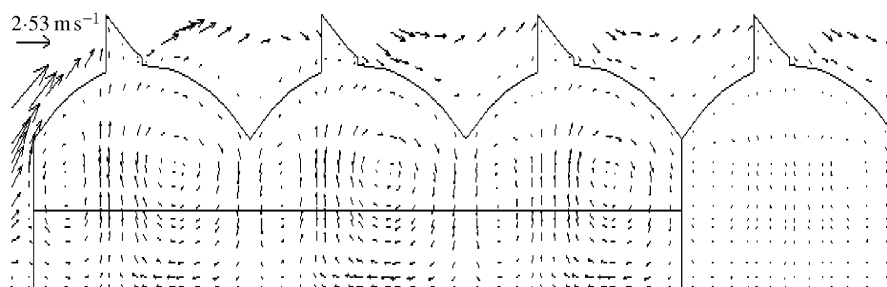


Fig. 11. Dynamic field within the greenhouse for the configuration with open windward and side openings and with anti-*Thrips* nets on the vents (inside horizontal line refers to crop height)

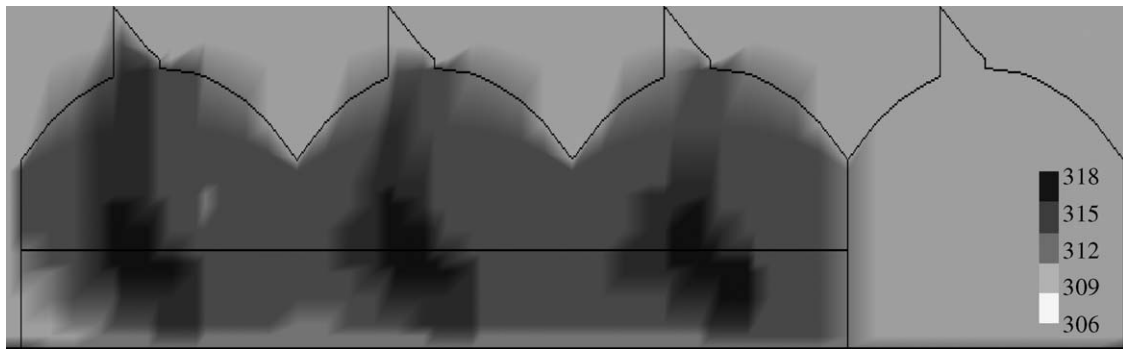


Fig. 12. Air temperature field in K within the greenhouse for the configuration with open windward and side openings and with anti-Thrips nets on the vents (inside horizontal line refers to crop height)

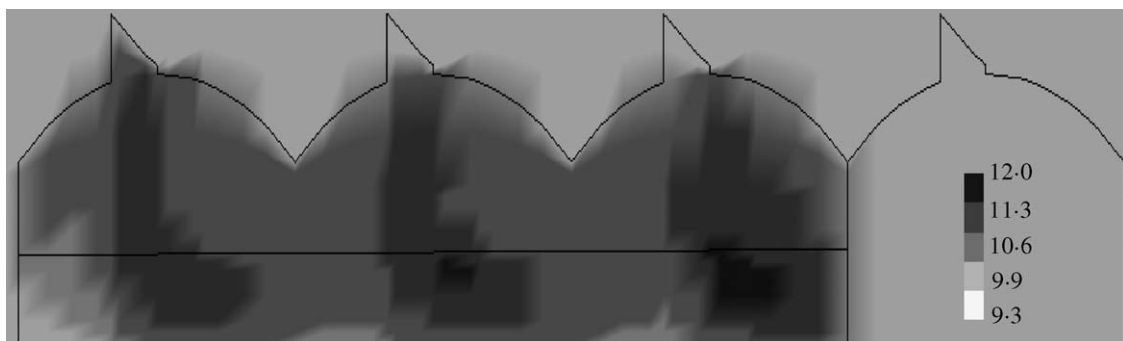


Fig. 13. Air humidity field in g kg^{-1} within the greenhouse for the configuration with open windward and side openings and with anti-Thrips nets on the vents (inside horizontal line refers to crop height)

References

- Bailey B J** (2000). Constraints, limitations and achievements in greenhouse natural ventilation. *Acta Horticulturae*, **534**, 21–30
- Boulard T** (2004). Modelling the distributed greenhouse climate at crop and leaf level. International Workshop: Agriculture Structures & Environmental Control, Suwon-city, Korea, 14–16 June
- Boulard T; Baille A** (1995). Modelling of air exchange rate in a greenhouse equipped with continuous roof vents. *Journal of Agricultural Engineering Research*, **61**, 37–48
- Boulard T; Baille A; Mermier M; Villette F** (1991). Measurement and modelling of greenhouse tomato leaves stomatal resistance. *Agronomie*, **11**, 259–274
- Boulard T; Mermier M; Fargues J; Smits N; Rougier M; Roy J C** (2002). Tomato leaf boundary layer climate: implication for microbiological control of whiteflies in greenhouse. *Agricultural & Forest Meteorology*, **110**, 159–176
- Boulard T; Wang S** (2002). Experimental and numerical study on the heterogeneity of crop transpiration in a plastic tunnel. *Computers and Electronics in Agriculture*, **34**, 173–190
- Boulard T; Wang S; Haxaire R** (2000). Mean and turbulent air flows and microclimatic patterns in an empty greenhouse tunnel. *Agricultural and Forest Meteorology*, **100**, 169–181
- CFD2000® Manual** (1997). CFD System, version 4.0. Pacific Sierra Corp., USA
- Fatnassi H** (2001). Modélisation du microclimat et de l'hétérogénéité climatique dans une serre de grande surface équipée de filets anti-insectes. [Microclimate modelling of a large scale greenhouse equipped with anti-insect screens on the openings.] PhD Thesis, University Ibn Zohr, Faculté des Sciences d'Agadir, Maroc, 169pp
- Fatnassi H; Boulard T; Bouirden L** (2003). Simulation of climatic conditions in full-scale greenhouse fitted with insect-proof screens. *Agricultural & Forest Meteorology*, **118**, 97–111
- Fernandez J E; Bailey B** (1992). Measurement and prediction of greenhouse ventilation rates. *Agricultural & Forest Meteorology*, **58**, 229–245
- Haxaire R** (1999). Caractérisation et Modélisation des écoulements d'air dans une serre. [Characterisation and modelling of the air flows within a greenhouse.] Thèse de Docteur en Sciences de l'Ingénieur de l'Université de Nice, Sophia Antipolis, 148pp
- Jones P J; Whittle G E** (1992). CFD for building air flow prediction-current capabilities. *Building & Environment*, **27**(3), 321–338
- Lauder B E; Spalding D B** (1972). *Mathematical Models of Turbulence*. Academic Press, New York
- Lee I; Short T H** (2000). Two-dimensional numerical simulation of natural ventilation in a multi-span greenhouse. *Transactions of the ASAE*, **43**(3), 745–753

- Mohammadi B; Pironneau O** (1994). Analysis of the $k-\varepsilon$ Turbulence Model, Research in Applied Mathematics. Wiley, Masson, USA
- Roy J C; Boulard T; Kittas C; Wang S** (2002). Convective and ventilation transfers in greenhouses, Part 1: the greenhouse considered as a perfectly stirred tank. Biosystem Engineering, **83**(1), 1–20
- Scruton C** (1981). An Introduction to Wind Effects on Structures. Oxford University Press, Oxford, UK
- Wilson J D** (1985). Numerical studies of flow through a wind break. Journal of Wind Engineering and Industrial. Aerodynamics, **21**, 119–154